Fall 1-31-2016

Triplex dna receptor-gold nanoparticle conjugates for detection of oxidized dna base

Qingyu Xing
New Jersey Institute of Technology

Copyright Warning & Restrictions

The copyright law of the United States (Title 17, United States Code) governs the making of photocopies or other reproductions of copyrighted material.

Under certain conditions specified in the law, libraries and archives are authorized to furnish a photocopy or other reproduction. One of these specified conditions is that the photocopy or reproduction is not to be "used for any purpose other than private study, scholarship, or research." If a, user makes a request for, or later uses, a photocopy or reproduction for purposes in excess of "fair use" that user may be liable for copyright infringement,

This institution reserves the right to refuse to accept a copying order if, in its judgment, fulfillment of the order would involve violation of copyright law.

Please Note: The author retains the copyright while the New Jersey Institute of Technology reserves the right to distribute this thesis or dissertation

Printing note: If you do not wish to print this page, then select "Pages from: first page # to: last page #" on the print dialog screen

ABSTRACT

TRIPLEX DNA RECEPTOR-GOLD NANOPARTICLE CONJUGATES FOR DETECTION OF OXIDIZED DNA BASE

by
Qingyu Xing

Oxidations of DNA nucleobases are believed to be one of the sources of aging and some age-dependent disease, such as cancer. Human body have various mechanisms to repair damaged DNA and base-excision-repair is one mechanism for removing those oxidized nucleobases. This mechanism processes in the cells by cutting the oxidized nucleobases from deoxyribose and letting them excrete though urine. Detection of those abnormal nucleobases in urine has been suggested as a convenient way of early cancer diagnosis. 5-OHU (5-hydroxyuracil), the oxidation product of cytosine, is one of those abnormal nucleobases and it potentially forms base pairs with all four DNA nucleobases, which may in the end cause mutation. In this project, a binding cavity for 5-OHU in triplex system was designed and triplex conjugated gold nanoparticles were synthesized. The melting temperature of the triplex DNA-GNP conjugates were 5-OHU concentration dependent, which demonstrated the potential of the system for colorimetric detection of urinary 5-OHU.

TRIPLEX DNA RECEPTOR-GOLD NANOPARTICLE CONJUGATES FOR DETECTION OF OXIDIZED DNA BASE

by
Qingyu Xing

A Thesis
Submitted to the Faculty of
New Jersey Institute of Technology
in Partial Fulfillment of the Requirements for the Degree of
Master of Science in Chemistry

Department of Chemistry and Environmental Science

January 2016

APPROVAL PAGE

DNA TRIPLEX-GOLD NANOPARTICLE COMPLEX FOR DETECTION OF OXIDIZED DNA BASE

Qingyu Xing

Dr. Edgardo T. Farinas, Advisor Chair/Associate Professor of Chemistry and Environmental Science, NJIT	Date
Dr. Haidong Huang, Committee Member, Co-advisor Senior Scientist, Quantum-Si Inc.	Date
Dr. Zafar Iqbal, Committee Member Research Professor of Chemistry and Environmental Science, NJIT	Date

BIOGRAPHICAL SKETCH

Author: Qingyu Xing

Degree: Master of Science

Date: January 2016

Undergraduate and Graduate Education:

- Master of Science in Chemistry,
  New Jersey Institute of Technology, Newark, NJ, 2016

- Bachelor of Engineering in Polymer Materials and Engineering,
  Beijing University of Chemical Technology, Beijing, People's Republic of China, 2013

Major: Chemistry

I asked my father,

“When did you quit painting?”

“1991.”

I asked my mother,

“Is that your finest work?”

“No. You are.”

Their sacrifice makes me what I am.

God, I miss them in this moment.

ACKNOWLEDGMENT

This thesis cannot be done without the help of Prof. Huang and Prof. Farinas. As my advisors, they gave me continuous help and were always there guiding me whenever I was in trouble. My thank you also goes to Prof. Iqbal for being my committee member.

I have encountered many problems when I managed to finish this thesis and Xun Gao and Peter Tlatelpa gave me a lot of help in my experiments.

I would also want to thank other guys in the lab, including Silu Shen, Han Jia, Yuchen Peng and Joydeep Chakraborty, all of you guys were here for me and gave me a lot valuable suggestion. And Dr. Xu in Department of Chemical, Biological & Pharmaceutical Engineering, who gave me access to his instruments for my melting tests and Dr. Chaudhery Mustansar Hussain in Department of Chemistry & Environmental Science, who gave me access to UV-1800 spectrometer so I can finish my UV study on the mixture.

TABLE OF CONTENTS

TABLE OF CONTENTS
(Continued)

Chapter **Page**

LIST OF TABLES

LIST OF FIGURES

LIST OF SYMBOLS

M	Molar
μM	Micromolar
nM	Nanomolar
mL	Milliliter
GNP	Gold nanoparticle
DNA	Deoxyribonucleic acid
Nm	Nanometer
PBS	Phosphate-buffered saline
SDS	Sodium dodecyl sulfate
OD_{260}	Optical density at 260nm

LIST OF DEFINITIONS

Buffer	A solution consisting of a mixture of a weak acid and its conjugate base, used for maintaining pH.
DNA duplex	Double-stranded DNA held in a double helix by AT and CG base pairing.
DNA triplex	Triple-stranded DNA wind around each other holding by TAT and CGC^+ base triads.
Gold nanoparticles	Gold(0) particles with a diameter in nano-scale.

CHARPTER 1

INTRODUCTION

1.1 Objective

About a century ago, people realized that genes carry the genetic information. People also realized that the self-assemble of different bases gives templates for protein synthesis. These bases match each other accurately, in that adenine matches thymine while guanine matches cytosine. These precisely matched base pairs are making sure that the genetic information can be passed from generation to generation.

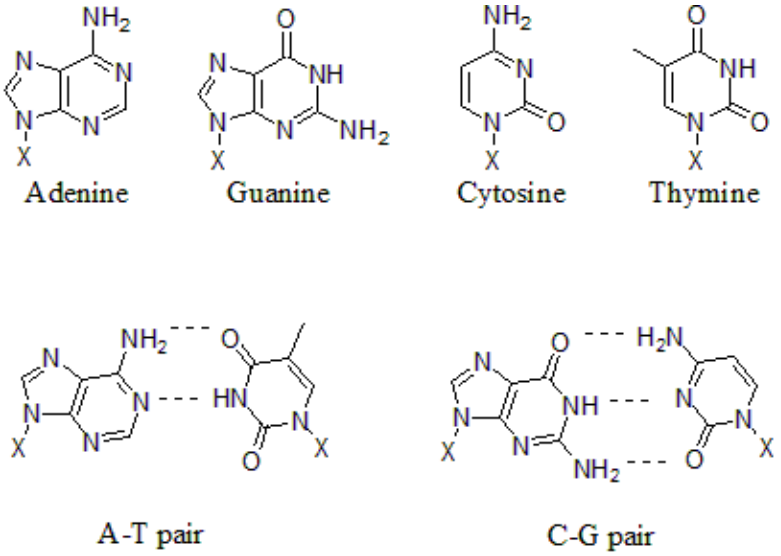

Figure 1.1 The structure of four DNA bases and the pairing of them, driving by specific hydrogen bonding, those bases self-assemble into specific base pairs, which are A-T pair and C-G pair.

Nevertheless, we are not all the same as our ancestor. We do not have tails or claws like they did. According to Darwin's theory, we become what we are though evolutions and they make us adapt to the environments better. Mutations of DNA chains

make evolution possible. DNA mutates randomly and the environment selects good mutations, in which life with these good mutations can stand the environment better, so that they can survive. Mutation happens all the time. Some viruses mutate very rapidly so they are hard to identify and track. However, humans are not as simple as viruses. Human body is a very complicated system. A small change in our body can be lethal, like the sickle cell trait. Within our body, DNA guides protein synthesis. It can be transcribed to mRNA, which is used as the template of protein synthesis. This process has its own regulations to make sure that our body synthesizes correct proteins in certain amounts. When a DNA chain contains a mistake, the cell may synthesize a malfunctioning protein, which lead to some diseases. If the mistake results in unregulated growth, it leads to cancer. Base substitution is a type of mutation. While some base substitution events are spontaneous, others are caused by damaging on bases, such as oxidation of DNA nucleobases. Oxidation of nucleobases occur when they react with reactive oxygen species (ROS) inside the cells[1-5]. The pairing preferences are changed when nucleobases are oxidized[6]. Examples of highly abundant oxidized bases include 5-hydroxyuracil[3], coming from oxidation of cytosine, and 8-oxoguanine[7], coming from oxidation of guanine.

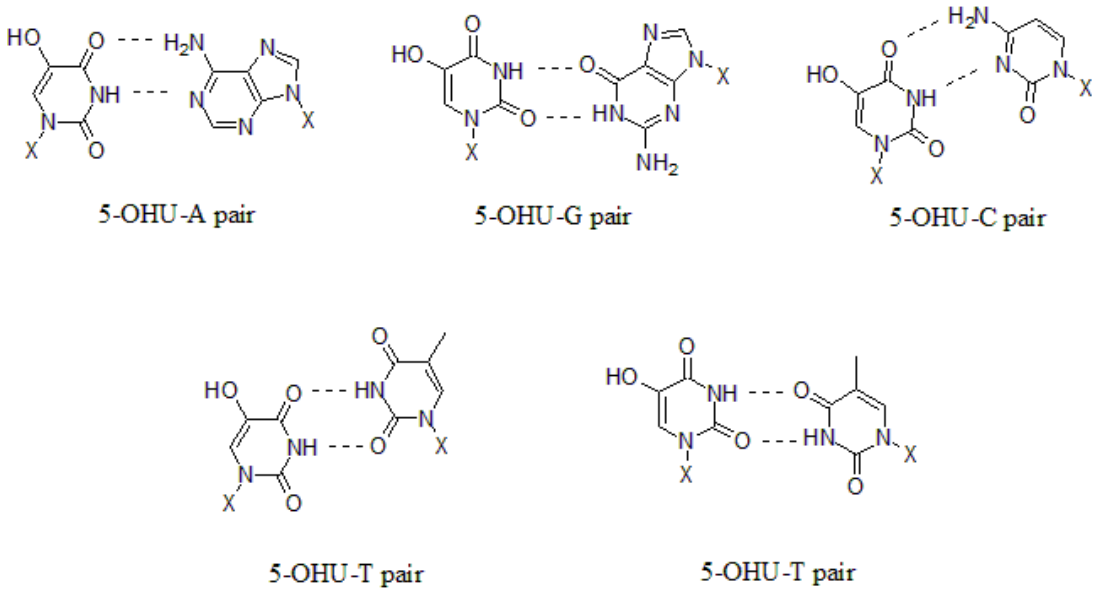

Figure 1.2 Gorenstein's group[3] indicates that 5-hydroxyluracil (5-OHU) can binds to all four DNA bases with different affinity. The 5-OHU-G pair is even more stable than a normal pair. With thymine, they suggest two ways of binding.

DNA damage is believed to be related to some diseases[2, 8-10]. To reduce the detrimental biological consequences caused by DNA damage, our body has developed various mechanisms to repair those damages[9]. One of these repair mechanisms, named base-excision-repair (BER), removes incorrect bases and replaces them with correct ones[10]. The damaged bases are released and excreted then can be detected in urine. Therefore the urinary concentration of those damaged bases can be a tool for evaluation of the *in vivo* DNA repair activities and possibly diagnosis of cancer[11].

Urinary nucleobases can be detected by many methods, like HPLC-MS or GC-MS[7, 12]. These methods require expensive instruments and trained professionals. As a result, they are not very convenient and can be very expensive. This diagnosis can be very simple if we can use a test kit, like the ones used for pregnancy test. All one needs to do is to take some urine sample and wait for the color to change. In this project, we want to find an assay that can generate color changing basing on the concentration difference

of 5-hydroxyuracil in the urine. To achieve this goal, first, we need to find a system to specifically recognize 5-hydroxyuracil, and secondly, this recognition needs to be accompanied with color changing.

DNA triplex, which is stabilized by TAT base triads and CGC^+ base triads, is a good candidate for this specific molecular recognition[13]. A few articles have been published in our lab on using triplex receptors for molecule detection[14, 15]. This method, comparing to others, have many advantages. On one hand, rational design of a DNA triplex binding site is much simpler than rational design of a protein binding pocket. On the other hand, nucleobase triplets in the triplex DNA system can provide very specific hydrogen bonding groups in a predictable geometry. In this project, we expanded the options of specific binding groups in triplex DNA receptors and designed a binding site based on metal-binding property of 5-hydroxyuracil and its extra hydrogen binding sites. The metal-binding interaction, as a strong interaction, are much stronger than a hydrogen bond. At the same time, 5-OHU, as a purine may not be favored in the middle of a triplex triad because of its geometry. A metal-recruiting modified base was synthesized and incorporated to an oligonucleotide chain, which was predicted to form a complex with 5-hydroxyuracil. Binding of 5-hydroxyuracil was expected to change the stability of the triplex and the change of stability can be reflected by the change of the melting temperature. This will generate a detectable signal when reporting groups are conjugated to the oligonucleotides.

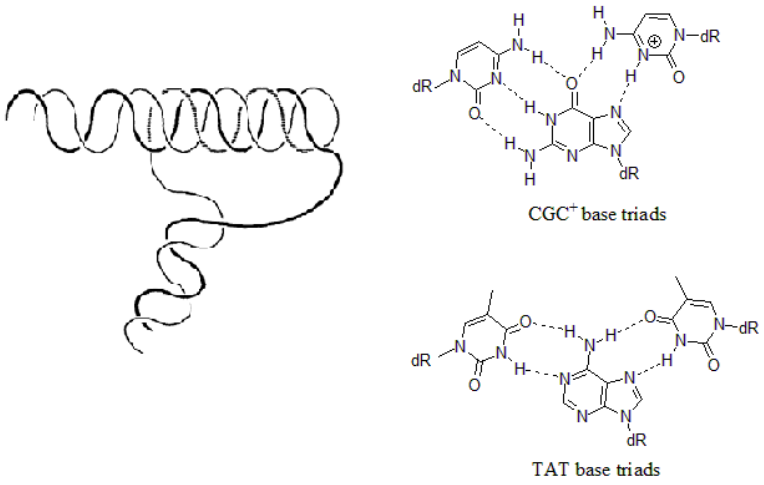

Figure 1.3 Left side: the structure of a triplex system, in which a single strand DNA binds to a duplex system at its major groove. Right side: the structure of TAT base triads and CGC^+ base triads[13].

When a material comes to a nano-scale, it shows a lot of different properties, which are because, on the nano-scale, the quantum theory starts to play an important role. Nanotechnology has been developed for many years and a lot of nanomaterials have been found. On the nano-scale, many materials show size-dependent properties. For example, gold nanoparticles show different melting points when their sizes differ[16]. At the same time, nano-scale is the scale of the wavelength of light. Materials show many size-dependent optical properties, such as the observation that fluorescent absorption and emission wavelengths of quantum dots differ by their sizes. Gold nanoparticles, also shows specific size-dependent optical properties. The color of gold nanoparticles varies with their sizes. With a size of about 10 nm, gold nanoparticles absorb light at wavelength of 520 nm and show ruby red, while they absorb light of longer wavelength and show a “bluer” color when the size increases[17-21]. This special property of gold nanoparticles makes them a good probe for analytical purposes[17, 18, 21-25].

The color of gold nanoparticles comes from surface plasmon of gold nanoparticles. Free electrons in the surface oscillates because light, as a polar electromagnetic field, drives them to. According to Rayleigh approximation of Mie theory[26], the absorbance of light can be given by

$$C_{abs} = k\alpha'' \tag{1.1}$$

In which,

$$\alpha = 4\pi R^3 \frac{N^2-1}{N^2+2} \tag{1.2}$$

In the equations above, R stands for radius of a nanoparticles, N is a material-dependent coefficient, k is wavenumber of light and C_{abs} is the cross-section of absorbance. This equation gives us an idea that the radius is proportional to the wavelength of light when cross-section is fixed. We can get a brief idea that when the size of gold nanoparticles get larger, they will absorb light with longer wavelength but the real situation is way complicated than this equation. Gold nanoparticles with a diameter less than 2 nm will not show any surface plasmon, as well as the bulky gold[19].

In this project, we attached ssDNA chains to gold nanoparticles. When the ssDNA chains self-assemble into a triplex system, as a result, gold nanoparticles form bigger clusters and result in the shift of wavelength of light absorbed. In another word, the color of DNA-conjugated gold nanoparticles suspension becomes “bluer” when DNA triplex forms and “redder” when DNA triplex “melts”. The gold nanoparticles that we are using have a diameter of about 13 nm, so they absorb light at a wavelength about 520 nm. When they are conjugated to DNA triplex, we can tell the melting point of DNA triplex system by testing its absorbance under different temperature.

Many research activities have been reported on using aptamers for molecular recognition with a visible signal generated by gold nanoparticles. Mirkin' group published an article to show using DNA duplex-conjugated nanoparticles for detection of cysteine[17]. In a simultaneously going project of our group, triplex-conjugated gold nanoparticles were used for detection of 8-oxoG. We found that with 8-oxoG in a urine sample, the melting temperature of the triplex increased. The sample with 8-oxoG remained purple after being incubated at a certain temperature. In contrast, the sample without 8-oxoG showed a red color.

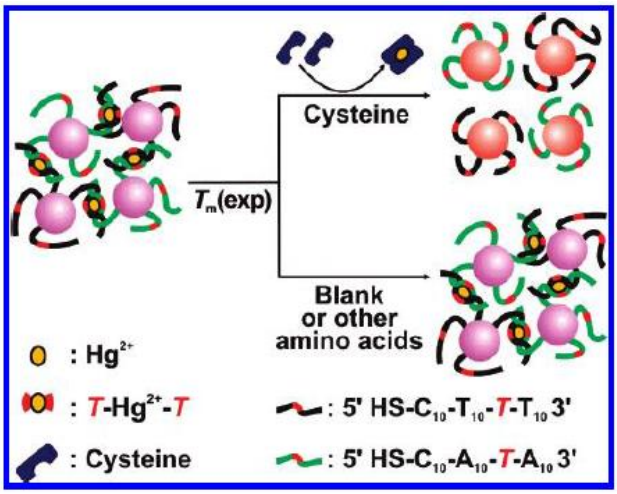

Figure 1.4 T-T base pairs bind to Hg^{2+} selectively which cysteine can extract Hg^{2+}out of T-T complex. The extraction results in decreasing of melting point and red color can be seen when incubating under certain temperature[17].

Source: Lee, J.-S., et al., *A DNA−Gold Nanoparticle-Based Colorimetric Competition Assay for the Detection of Cysteine.* Nano Letters, 2008. **8**(2): p. 530.

CHARPTER 2

SYNTHESIS OF OLIGONUCLEOTIDES CONJUGATED GOLD NANOPARTICLES AND MELTING TEST

2.1 Pathway of Pyridylpyrimidine Phosphoramidite Synthesis

Pyridylpyrimidine is the artificial nucleobase that we will use to recruit metal ions to the receptor binding cavity. Here the pathway of the synthesis of pyridylpyrimidine phosphoramidite is shown (Figure 2.1).

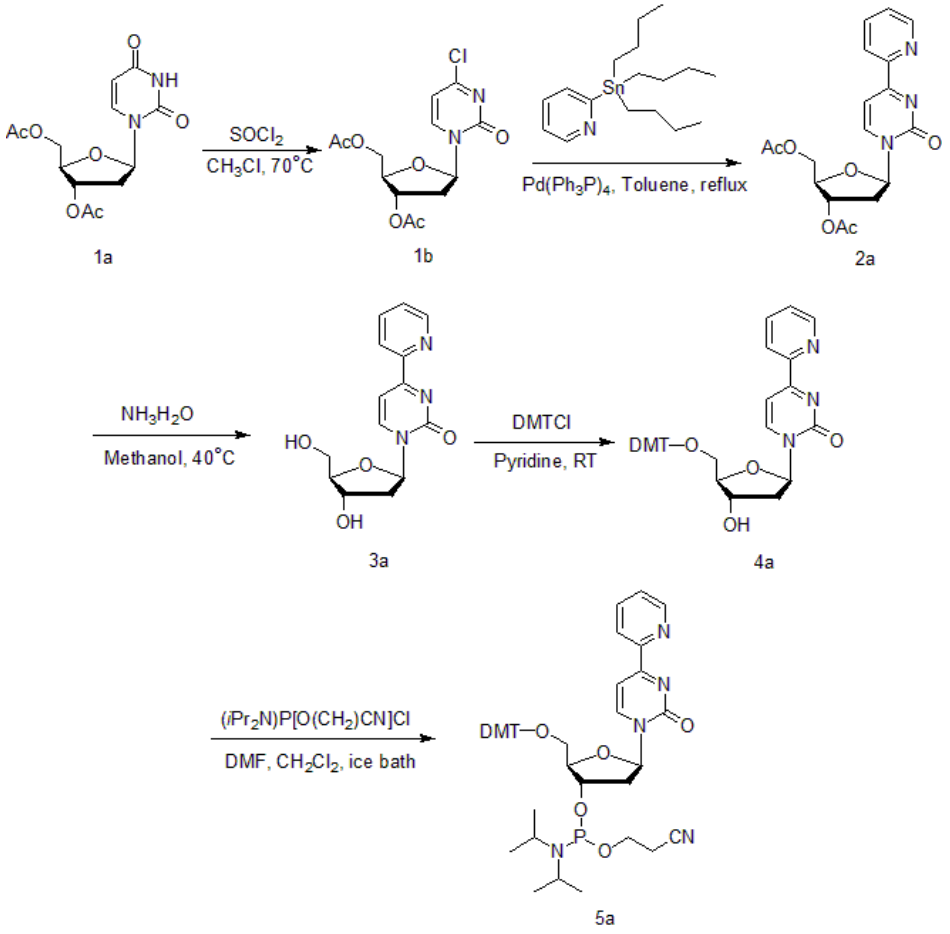

Figure 2.1 The pathway of synthesis of pyridylpyrimidine phosphoramidite.

The synthesis started from 3',5'-di-*O*-acetyl-2'-deoxyuridine (**1a**), which was prepared from 2'-deoxyuridine in the former work of our group. With the acetyl

protecting group on the 3’ and 5’-oxygen of the deoxyribose, molecule 1a does not have an active hydrogen so that it can undergo a chlorination reaction with thionyl chloride. This reaction turned out to be very sensitive to water, although thionyl chloride was in large excess and can remove water from the system. It was discovered during another project that our argon gas line contained a considerable amount of water vapor. By increasing the amount of thionyl chloride and controlling the quenching temperature very carefully with an ice bath, this reaction was finished in a high yield.

To connect a pyridine ring to the pyrimidine ring, the critical step was from **1b** to **2a**, which was a modified Stille coupling reaction. Under the catalysis of Pd(0), the pyridyl group was transferred to pyrimidine from 2-(tri-n-butylstannyl)pyridine. Compared to the uracil ring in the starting material, the pyridylpyrimidine adopts a significant resonance where the 3-nitrogen is an imine form, in which this nitrogen will no longer act as a hydrogen donor. However, its unpaired electrons become coplanar with the unpaired electrons of the pyridine nitrogen, which together create a good bind site for metal ions.

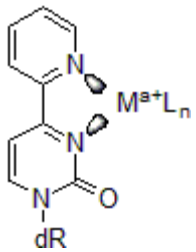

Figure 2.2 The unpaired electrons are in the same plane with the unpaired electrons in pyridyl group, which makes this base a good ligand for metal binding.

Dongwon’s study showed that this structure can act like a base pair[27]. Instead of hydrogen bonds normally found in the duplex DNA, coordinate bonds are here formed to hold the two bases together. Therefore in our work, starting from the conversion of **2a**

to **3a**, we tried our best avoiding metal ions throughout the synthesis. For example, sea sand used for column chromatography was washed with EDTA three times, followed by deionized water, before use.

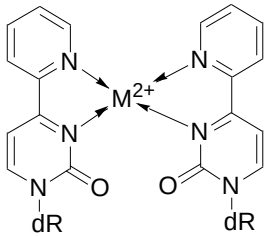

Figure 2.3 The complex formed by two pyridylpyrimidine and a metal ion in the middle. This structure can held this two bases together, which is just like hydrogen bonds do in a tranditional A-T or C-G pairs[27].

Formation of **3a** was confirmed by comparing the TLC (methanol to methylene chloride, 3 to 1, R_f=0.4) result of the product with a reference compound synthesized by a former graduate student in the lab, and this reference compound was previously confirmed by ^{1}H NMR. Formation of **2a** and **3a** was further confirmed by the fact that they had fluorescence emissions under long wavelength UV light. We experienced some difficulties in the synthesis of the phosphoramidite (**5a**). Although we confirmed the structure of **5a** by ^{1}H NMR, the yield seemed extremely low (9.9%). The same reaction carried out by another student in our lab showed that the starting material (**4a**) contained multiple triethylammonium and pyridinium salts. Therefore the low yield step was perhaps a result of overestimated tritylation yield (**3a** to **4a**).

2.2 Experimental

Chemicals from commercial purchase were used without further purification, useless otherwise described. UV spectra were recorded on a UV-1700 or UV-1800

spectrophotometer (Shimadzu). Gold nanoparticles is obtained from Dr. Xu's lab and used without further purification. UV-vis melting tests were done with a Cary 300 UV-vis spectrometer.

2.2.1 Synthesis of 1'-(2-oxo-4-chloropyrimidyl)-3', 5'-diacetyl-2'-deoxyribose (1b)

3', 5'-di-O-acetyl-2'-deoxyuridine was previously prepared in the lab. Chloroform was treated with calcium hydride overnight and distilled before use. Thionyl chloride was distilled before use. Compound **1a** (424 mg) was placed in a 50 mL single-neck round flask with a condenser and 15 mL of chloroform was injected from the top of the condenser. After all solid were dissolved, 1 mL of thionyl chloride and 0.09 mL of DMF were injected. The reaction was then heated with a preheated 70 ˚C oil bath for 100 min under argon. The oil bath was removed and the reaction was slowly cooled to room temperature under argon. The mixture was further cooled to 0 ℃ in an ice bath. Then the condenser was removed and saturated sodium bicarbonate solution was added slowly and very carefully to avoid a significant change of temperature until gas stopped evolving. Methylene chloride (15 mL) was added. The organic layer was separated and washed successively with saturated sodium bicarbonate solution (2 x 15 mL) and saturated sodium chloride solution (2 x 15 mL). The solvent was evaporated and the residue was purified by column chromatography (pure methylene chloride then 1% methanol) to yield **1b** (322 mg, yield: 71.7%). Compound **1b** was an oil-like product under vacuum but solidified in atmosphere.

2.2.2 Synthesis of 1'-(2-oxo-4-pyridylprymidyl)-3', 5'-diacetyl-2'-deoxyribose (2a)

Toluene was distilled with metal sodium before use. Took out 15 mL of toluene and bubbled it with argon followed by injecting 0.3 ml 2-(tri-n-butylstannyl)pyridine. Compound **1b** was placed in a 50 mL flask and 50 mg of tetrakis(triphenylphosphine)palladium(0) was added. The flask was connected with a condenser and replaced gas with argon for three times. The 2-(tri-n-butylstannyl)pyridine toluene solution was injected under argon pressure. The mixture was refluxed under argon for 16 hours. The mixture turned to dark red after a while. After 16 hours, removed the oil bath and cooled the mixture down to room temperature slowly and 20 ml of deionized water was added. Inorganic phrase was collected and extracted with 20 mL of ethyl acetate for four times. Removed the solvent and purify the residues with column chromatography. In the end, 194 mg (yield: 44.3%) of compound **2a** was obtained.

2.2.3 Synthesis of 1'-(2-oxo-4-pyridylprymidyl)-2'-deoxyribose (3a)

To the flask contained **2a**, 10 mL methanol was added. After everything was dissolved, transferred the solution to a pressure reactor. To the reactor, 10 ml of ammonia hydroxide was added. The reactor was sealed and incubated under 40 ˚C overnight. The mixture was cooled down in refrigerator for 30 minutes then dried with speedvac. 156 mg brown solid was obtained followed by purified with column chromatography. 92 mg (yield: 64.2%) of compound **3a** was obtained.

2.2.4 Synthesis of 1'-(2-oxo-4-pryidylpyrimidyl)-5'-(4, 4'-dimethoxytriphenylmethyl) -2'-deoxyribose (4a)

Pyridine was dried with sodium hydroxide overnight and distilled before use. To a single neck flask, 101 mg 4, 4'-dimethoxytriphenylmethyl chloride was added and dissolved with pyridine under argon. Replaced the air in the flask with argon for three times. The 4, 4'-dimethoxytriphenylmethyl chloride pyridine solution was transferred to the flask under argon. The mixture then incubated under room temperature for five hours, monitored with TLC (methylene chloride to methanol 15 to 1) and extra 15 mg 4, 4'-dimethoxytriphenylmethyl chloride was added. The mixture was cooled down in ice bath followed by adding 2 mL of methanol slowly and carefully to quench. All the solvent was removed with rotavap in a mild condition. The temperature of the evaporation should be no more than 30 ˚C. Residues are purified with column chromatography. 103 mg (yield: 58.9%) compound **4a** was obtained.

2.2.5 Synthesis of 1'-(2-oxo-4-pyridylprymidyl)-2'-deoxyribose Phosphoramidite (5a)

Methylene chloride was dried overnight with calcium hydride and distilled before use. The flask contains **4a** was replaced with argon for three times. Because the product is very sensitive to oxygen. To the flask, 5 mL methylene chloride was added followed by adding 0.1 mL of DIPEA (N, N-diisopropylethylamine). The mixture was then stirred in ice bath, while 0.07 ml of CDP (2-cyanoethyl N, N-diisopropylchlorophosphoramidite) was transferred to the flask quickly under argon. The mixture was incubating for another 3 hours. Removed the solvent in mild condition and purified the residues with column chromatography. 14 mg compound **5a** (yield: 9.9%) was obtained.

2.2.6 Synthesis of Oligonucleotides

Oligonucleotides were synthesized on an ABI 394 solid phase oligonucleotide synthesizer. Three strands of DNA oligonucleotides were synthesized. The sequences were

5'-GCTCAACCTTCTCTATCTTCTTC-PEG-SH-3' (strand A),

5'-GAAGAAGAC$_3$AGAGAAGGTTGAGC-3' (strand B),

5'-CCTCCTCT*p*TCTCTTCC-PEG-SH-3' (strand C),

In which C_3 stands for a C_3 spacer and PEG stands for polyethylene glycol. Both A-strand and C-strand have a thiol group on 3' end for conjugating with gold nanoparticles. After the synthesis was finished, the strands were cleaved from solid surface by incubating the resin with ammonia at 55℃ overnight. The ammonia was removed by a speedvac and the remaining oligonucleotides were extracted by denaturing buffer and purified by denaturing PAGE. The oligonucleotides bands were cut form the gel, smashed, and extracted in a buffer containing 1 M NaCl and 1 mM tris-EDTA (pH 7.5). The extracts were passed through C18 cartridges and dried in a speedvac. The residues were redissolved in autoclaved water.

2.2.7 Synthesis of DNA Conjugated Gold Nanoparticles

The gold nanoparticles were previously prepared in Dr. Xu's lab, with a diameter of 13 nm and concentration of 17 nM. Conjugating of oligonucleotides and gold nanoparticles was enabled by forming coordination bonds between the gold nanoparticle surface and the thiol groups on the oligonucleotides. To a tube contains 10 nmole of oligonucleotide, 10 μL DTT (dithiothreitol, dissolved in 0.17 M PBS buffer, pH 8) was added and the

resulting solution was incubated for 1 h to cleave the disulfide bond in the 3'-end of the oligonucleotides. The mixture was purified by NAP-5 columns, eluted with deionized water. OD_{260} of eluted oligonucleotides were measured with a UV spectrometer and 1.7 OD_{260} of nucleotides were obtained. For every OD_{260} of oligonucleotides, 2 mL of gold nanoparticle suspension was added. The mixture stood at room temperature overnight. Equation 2.1 is used for calculation of OD_{260}.

$$\mathrm{OD}_{260} = A \times \frac{V_s}{V_c} \times f \tag{2.1}$$

To the oligonucleotide-GNP mixture, 34 μL 10% SDS and 340 μL 0.1 M PBS buffer (pH 7.4) were added to reach a final solution containing 0.1% SDS and 0.01 M PBS (pH 7.4). Resulting solution was incubated at room temperature for 20 min. Added 340 μL 200mM NaCl (dissolved in 0.1% SDS, 0.01 M PBS, pH 7.4) to the solution, followed by incubating for 2 hours. This process was repeated for three times until all 1020 μL 200mM NaCl (dissolved in 0.1% SDS, 0.01 M PBS, pH 7.4) was added to the system. The suspension then was allowed to stand at room temperature for 2 days.

2.2.8 Fluorescence Titration of Pyridylpyrimidine Nucleoside with Cu^{2+}

Fluorescence titration of **3a** was done with recording the intensity at 419 nm. To a fluorescence spectroscopy cuvette contained 500 μL 5 μM **3a**, 100 μM $CuSO_4$ was added 2.5 μL time by time and the fluorescence intensity at 419 nm was recorded. After the Cu^{2+} concentration reached 7.5 μM, started to add 1 mM $CuSO_4$, 1.25 μL at a time. The fluorescence intensity at 419 nm was recorded after every time of adding.

2.2.9 UV Study of Pyridylpyrimidine Nucleoside (3a), Cu^{2+} and 5-OHU Mixture

To a UV-vis spectroscopy cuvette contains 2.5 mL 20 μM **3a**, 1 mM of $CuSO_4$ was added, 5 μL at a time. The absorbance at 348.8 nm was recorded after each adding. When Cu^{2+} concentration reached 44 μM, 100 μM of 5-OHU was added, 50 μL at a time. The absorbance at 348.8 nm was recorded after each adding.

In the second round of experiment, to a UV-vis spectroscopy cuvette, 400 μL 100 μM **3a**, 400 μL 100 μM $CuSO_4$ and 1.2 mL deionized water was added and the absorbance at 348.8 nm was recorded. Increasing the concentration of 5-OHU with 1000 μM 5-OHU solution and recorded absorbance at 348.8 nm for every concentration.

2.2.10 Melting Test of Triplex-Conjugated Gold Nanoparticles

Starting temperature of melting testing was 10 ˚C, ending temperature was 60 ˚C, holding time was 30 min and heating rate was 0.5 ˚C/min. Absorbance data was recorded every one minute and the melting temperature was obtained with first derivative method.

For each melting sample, 130 μL of DNA conjugated gold nanoparticles was took and washed 3 times with centrifuge. In each time of washing, the suspension was centrifuged with 13,000 rpm for 20 min. Then the supernatant was removed with a pipette, and the residue was redispersed in 130 μL 0.01 M PBS buffer (PBS 0.01 M, NaCl 0.1 M, SDS 0.1%, pH 7.4). Sonicate the suspension for 10 s to break the aggregation when any participates were observed during the redispersion steps.

To a 1.5 mL tube, 120 μL washed A strand conjugated gold nanoparticles suspension, 120 μL washed C strand conjugated gold nanoparticles suspension, 16 μL 10 μM B strand solution (dissolved in 0.01 M PBS buffer with 0.1 M NaCl and 0.1% SDS)

and 8 μL 1 M $MgCl_2$ solution was added. $CuSO_4$ and 5-OHU solutions (dissolved in 0.01 M PBS buffer with 0.1 M NaCl and 0.1% SDS) with concentrations of 50 μM and 100 μM were used to adjust the Cu^{2+} and 5-OHU concentrations in the final solutions. Brought the volume in every tube to 800 μL with 0.01 M PBS buffer (0.01 M PBS, 0.1 M NaCl and 0.1% SDS). The tubes were shielded with alumina coil and allowed to stand for 2 days before used for UV-vis melting test. The DNA-conjugated gold nanoparticles are very sensitive to ion strength; instantaneously local ion strength changing would result in breaking down of the system.

CHAPTER 3

RESULTS AND DISCUSSION

3.1 Fluorescence Titration of Pyridylpyrimidine Nucleoside with Cu^{2+}

We first examined the metal binding ability of **3a**. Nucleoside **3a** absorbs light at 328 nm and emits light with a peak at 419 nm. When 3a formed complex with Cu^{2+}, its fluorescence was quenched. Specifically, a $CuSO_4$ solution was titrated into to a solution containing 5 μM of **3a**.

Assuming that the binding of Cu^{2+} to **3a** is a one-to-one binding event and Cu^{2+} is in large excess, the Cu^{2+} concentration can be thought of remaining the same. The dissociation equation process is shown below, in which L stand for **3a** and K_d is the dissociate constant.

$$(CuL)^{2+} \overset{K_d}{\rightleftharpoons} Cu^{2+} + L$$

In which,

$$K_d = \frac{[Cu^{2+}][L]}{[(CuL)^{2+}]} \tag{3.1}$$

Although the free nucleoside concentration cannot be directed measured, its total concentration is known, named $[L]_t$, in which,

$$[L] + [(CuL)^{2+}] = [L]_t \tag{3.2}$$

Therefore,

$$\frac{[(CuL)^{2+}]}{[L]_t} = \frac{[Cu^{2+}]}{K_d + [Cu^{2+}]} \tag{3.3}$$

During the fluorescence titration, forming of complex results in fluorescence quenching until the intensity of fluorescence stops decreasing when the Cu^{2+}

concentration reached a certain level. The decrease of intensity is proportional to the portion of the nucleoside that has been converted to the complex. Accordingly, the largest difference in intensity would be a result that all the 3a molecules have been converted complexes. Therefore, $[(CuL)^{2+}]/[L^{2+}]$ in theory has the same value as $\Delta F/\Delta F_{max}$, in which ΔF is the intensity difference and ΔF_{max} is the largest intensity difference. An abnormal constant A was added to indicate how much the model is different from the real case (equation 3.4).

$$\frac{\Delta F}{\Delta F_{max}} = \frac{A[Cu^{2+}]}{K_d + [Cu^{2+}]} \tag{3.4}$$

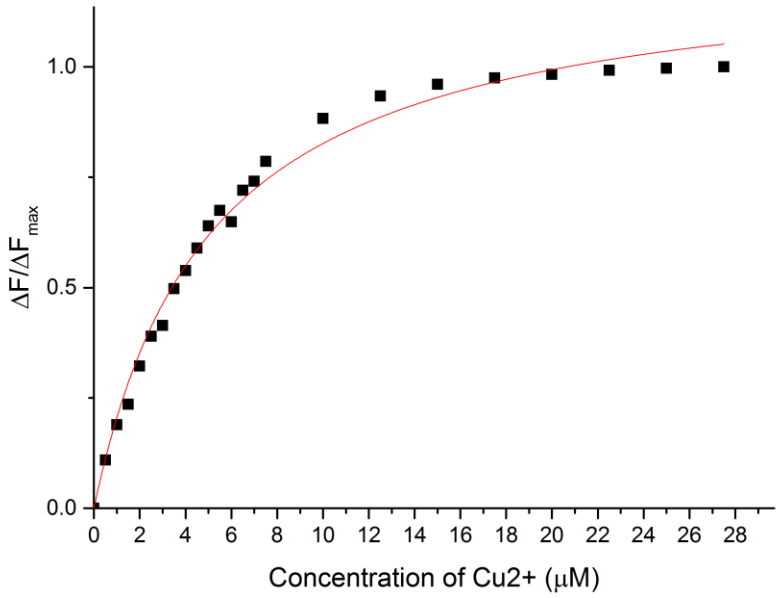

Figure 3.1 The data got from fluorescence quenching titration, in which black dots are the raw data and red line is the fitted curve.

Table 3.1 The Data Obtained from Fluorescence Quenching Titration

Concentration of Cu^{2+} (μM)	**Fluorescence intensity at 419 nm**	**ΔF**	**$\Delta F/\Delta F_{max}$**
0	538	0	0.000
0.5	483	54	0.109
1	443	94	0.189
1.5	420	117	0.235
2.0	377	160	0.322
2.5	344	193	0.389
3	332	206	0.414
3.5	290	248	0.498
4	269	268	0.539
4.5	244	293	0.589
5	219	318	0.640
5.5	202	336	0.675
6	214	323	0.649
6.5	179	358	0.720
7	169	369	0.741
7.5	146	391	0.786
10	98	440	0.883
12.5	73	465	0.934
15	59	478	0.961
17.5	52	485	0.975
20	48	489	0.983
22.5	44	494	0.992
25	43	495	0.994
27.5	41	496	0.997
30	40	498	1.000

We fit the data above into equation (3.4) with Originlab, which gave,

$$\frac{\Delta F}{\Delta F_{max}} = \frac{1.2*[Cu^{2+}]}{4.9+[Cu^{2+}]} \quad (3.5)$$

R^2 of this fitting was 0.9881. K_d equaled to 4.9 μM. A equaled to 1.2, which suggested that our model was close to the real case.

This titration experiment gave us a brief idea about the concentration of Cu^{2+} required for effective 5-OHU detection. However, this model was not completely accurate because when the concentration of Cu^{2+} was very low, the assumption that free Cu^{2+} concentration equals to the total Cu^{2+} concentration was clearly incorrect. In addition, the formation of **3a**-Cu-**3a** ternary complex cannot be ruled out. Another factor that was not taken into account was the pH effect, which would affect both the strengths of the ligand donor and the Cu^{2+} acceptor in a non-buffered system. However, it is apparent that upper nanomolar or lower micromolar concentrations of Cu^{2+} would be required to build a metal-containing triplex DNA system.

3.2 The UV Study of Pyridylpyrimidine Nucleoside, 5-hydroxyuracil and Cu^{2+} Mixture

After we obtained the estimation of binding constant between **3a** and Cu^{2+}, we sought to study the ternary complex formed by **3a**, 5-OHU, and Cu^{2+}. However, 5-OHU does not have significant fluorescence emission. Therefore fluorescence quenching is not a choice to study the binding between 5-OHU and Cu^{2+}. Unlike pyridylpyrimidine, whose UV spectrum was dependent on the concentration of Cu^{2+} in the solution (discussed later), the UV spectrum of 5-OHU did not change in the presence of Cu^{2+}. Therefore direct measure of binding between 5-OHU and Cu^{2+} using UV-vis titration was not viable. An alternative approach was to titrate 5-OHU into the complex between **3a** and Cu^{2+}, although the system would be more complicated and require careful analysis. When we added 5-OHU into a solution containing **3a** and Cu^{2+}, there were three possibilities. First, 5-OHU was a much better ligand than **3a**, and it would compete with **3a** for binding Cu^{2+} even at low

concentrations, resulting in the formation of 5-OHU-copper complex and immediate drop of the absorbance of **3a**-Cu^{2+} complex ; second, 5-OHU was a very weak ligand, so it will not influence the binding between **3a** and Cu^{2+} at concentrations relevant to the study; finally, 5-OHU is a ligand for Cu^{2+} with a similar binding constant as **3a**, and it would like to form a ternary complex containing **3a**, Cu^{2+} and 5-OHU itself first, then displaced **3a** completely.

1. The 5-OHU and Cu^{2+} binding was stronger than 3a, resulted in decrease of the **3a**-Cu^{2+} complex concentration.

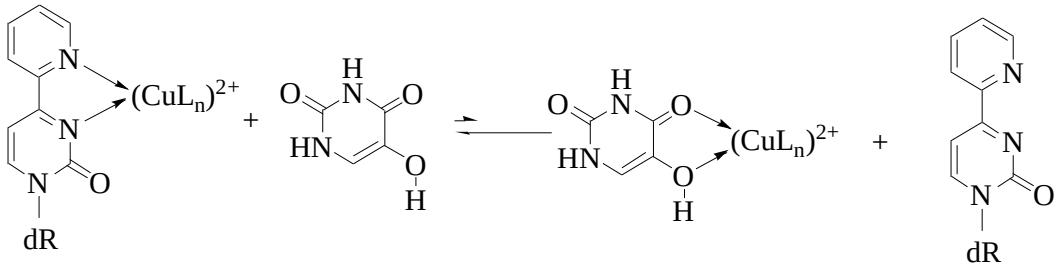

2. The binding of 5-OHU to Cu^{2+} was very weak, so 5-OHU would not influence the binding of **3a**.

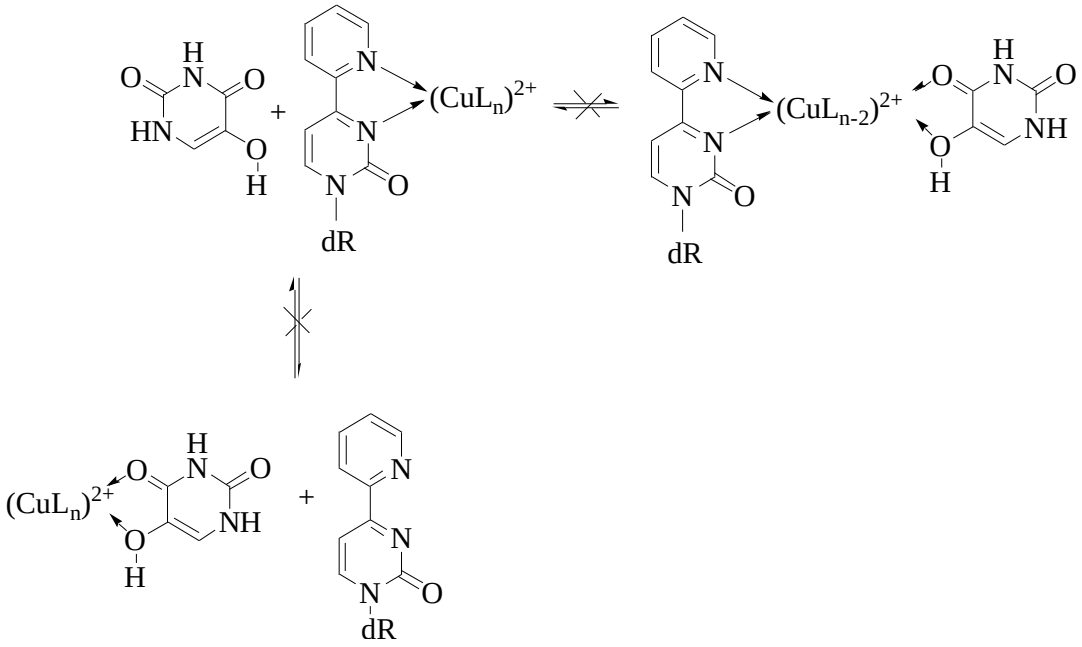

3. The binding of 5-OHU was a good ligand for Cu^{2+} and it was likely to form a ternary complex containing **3a**.

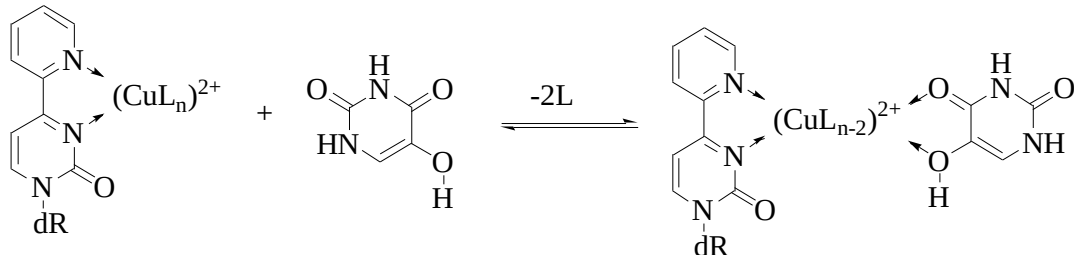

First, we recorded the UV spectra of 20 μM **3a** and started to add $CuSO_4$ solution to it and recorded the UV spectra at different Cu^{2+} concentration (from 0 to 44 μM). We found that the UV of peak at 327.5 nm shifted with the presence of Cu^{2+}, which indicates the forming of **3a**-Cu^{2+} complex.

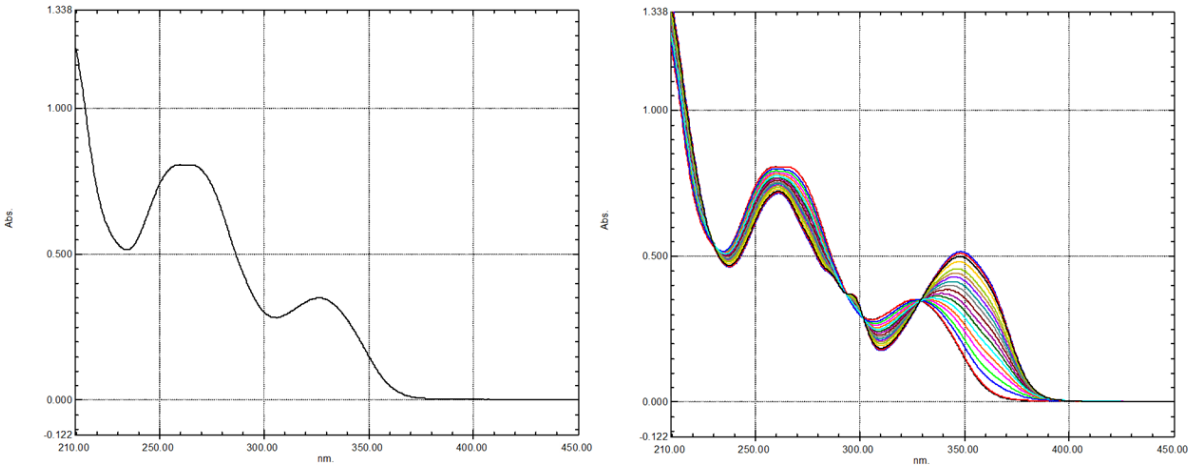

Figure 3.2 The UV spectrum of **3a**, on the left is the UV spectrum of **3a** in water solution, the UV spectrum of **3a** have two peaks at 267.5 nm and 327.5 nm. On the right side shows the peak shifting with the concentration increasing of Cu^{2+}. The concentration of **3a** in both case is 20 μM and the concentration of Cu^{2+} in the right graph changes from 0 μM to 44 μM. After 44 μM of Cu^{2+} is reached, the peak shift from 327.5 nm to 348.2 nm. The shifting of the peak at 327.5 nm indicates the complex forming when Cu^{2+} is added to the system.

We added 5-OHU into the system containing 20 μM of **3a** and 44 μM of Cu^{2+}, and recorded the UV spectrum at different 5-OHU concentration (from 0 to 20 μM). The peak at 348.2 nm decreased with the concentration of 5-OHU increasing but the change was not significant.

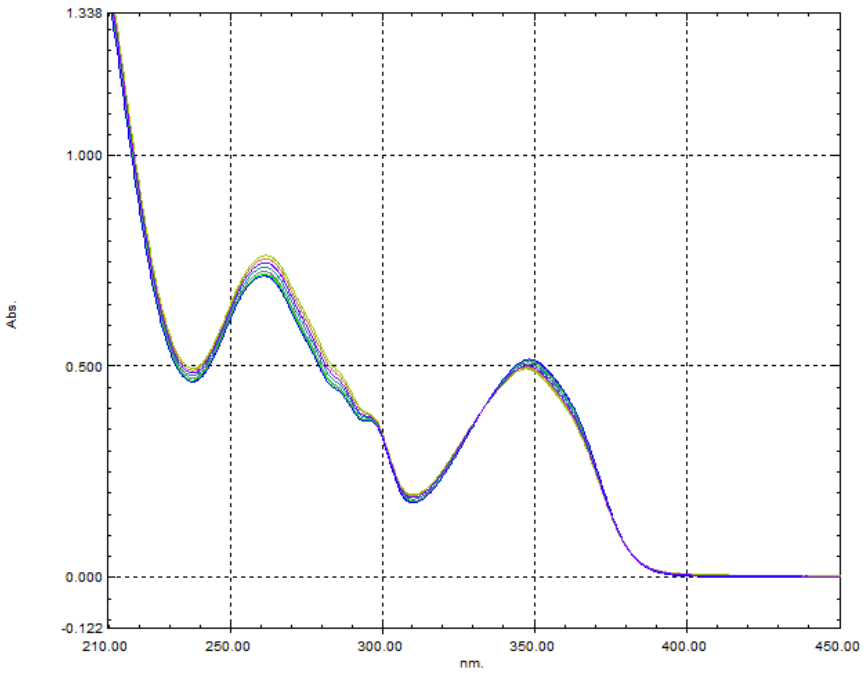

Figure 3.3 The peak changing when added 5-OHU to a system contains 20 µM **3a** and 44 µM Cu^{2+}. The peak at 348.2 nm drops with the concentration of the concentration of 5-OHU increases.

Another set of experiment was done by adding 5-OHU into a solution containing 20 µM Cu^{2+} and 20 µM of **3a**, the UV spectra was recorded with different 5-OHU concentrations, ranging from 0 to 200 µM. The absorbance at 348 nm also dropped but still not very significant. Comparing to the former experiment, in which the absorbance drop was 0.022 unit at 44 µM of 5-OHU, this set of experiments showed a more significant absorbance drop of 0.043 unit at 48 µM of 5-OHU. This indicates that with less free Cu^{2+} in the solution, the same amount of 5-OHU had more influence on the UV spectra of **3a** and Cu^{2+} complex. The resulting product was clearly a ternary complex rather than the 5-OHU-Cu^{2+}, because a new peak appeared centering at 332 nm, which was much longer than the wavelength of 5-OHU-Cu^{2+} complex. By bringing the concentration of 5-OHU to 10 folds of **3a**, which was 200 µM, we saw that the peak at 332 nm also decreased. The result was liked caused by displacement of the **3a**-copper-5-

OHU ternary complex by 5-OHU-copper-5-OHU complex. This result gave us a reason to believe that the ternary complex among **3a**, 5-OHU, and Cu^{2+} indeed existed.

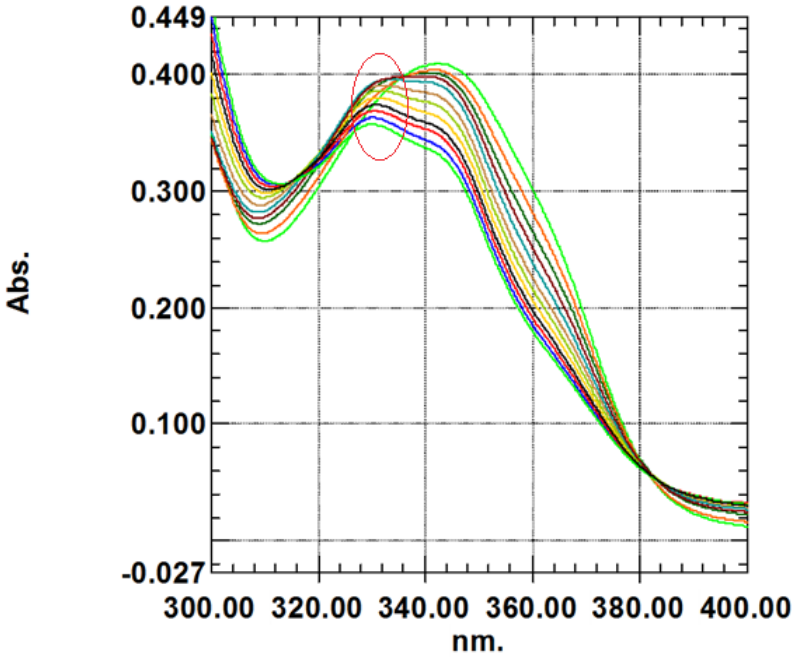

Figure 3.4 Titration of **3a**-Cu^{2+} complex with 5-OHU. Concentrations, 20 μM **3a**, 20 μM, Cu^{2+}.

3.3 The Melting Test of Triplex DNAReceptors Conjugated with Gold Nanoparticles

The forming of triplex DNA is a driving force for gold nanoparticles to aggregate, while the melting of triplex system results in the dissociation of the GNP aggregates. This process can be monitored by recording the absorbance at 520 nm. The UV-vis melting experiments were carried out by recording the response of A_{520} (absorbance at 520 nm) to temperature changes. The melting temperature was determined by the first derivative method, which determined the temperature at which the first derivative of A_{520} meets its maximum.

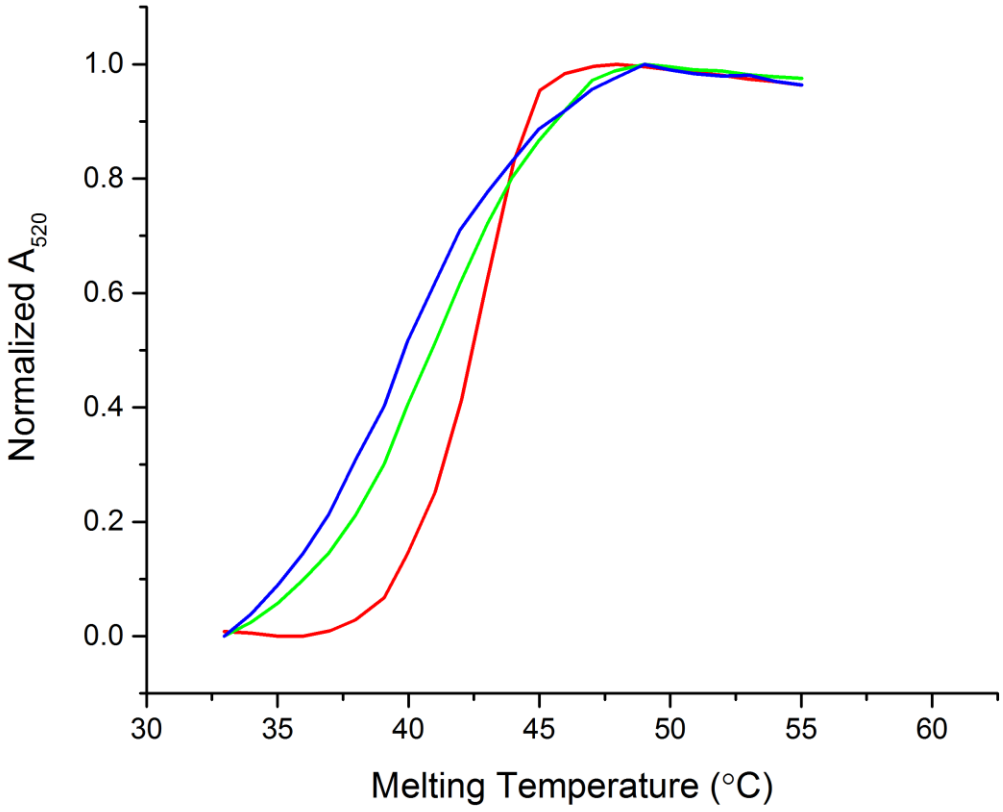

Figure 3.5 The melting curves. Red, 10 mM PBS, 100 mM NaCl, 10 mM $MgCl_2$, 0.1% SDS, 100 nM DNA, 2 μM Cu^{2+} and 0.4 μM 5-OHU; Blue, 10 mM PBS, 100 mM NaCl, 10 mM $MgCl_2$, 0.1% SDS, 100 nM DNA, 2 μM Cu^{2+} and no 5-OHU; Green, 10 mM PBS, 100 mM NaCl, 10 mM $MgCl_2$, 0.1% SDS, 100 nM DNA, 2 μM Cu^{2+} and 1 μM of 5-OHU.

The melting experiments were first carried out in 10 mM PBS buffer (pH 7.4). However, we found that the results were very inconsistent with each other and the errors were very large.

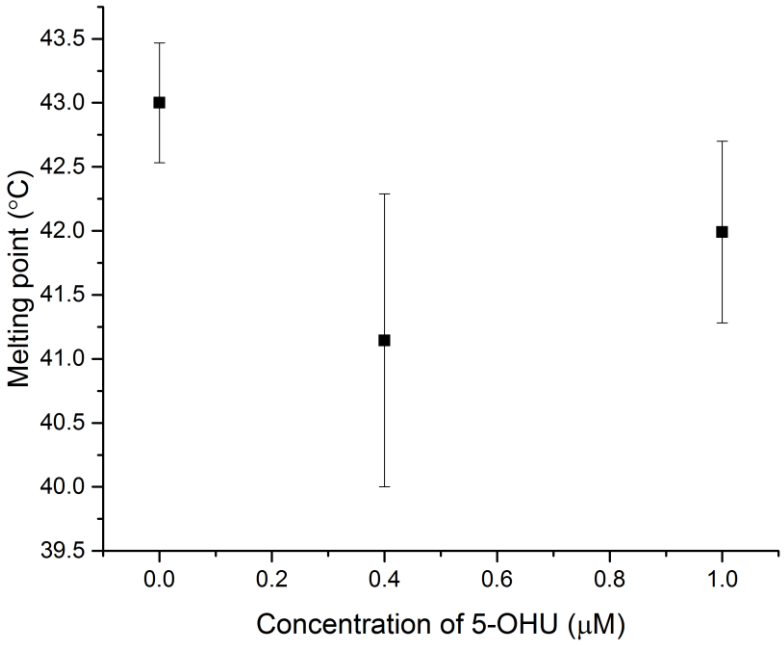

Figure 3.65 The melting test results with 100 nM of DNA, 10 mM of PBS buffer, pH 7.4, 10 mM of $MgCl_2$, 100 mM of NaCl, 0.1% of SDS (by weight) and 2 μM of Cu^{2+}. The errors of those data are very big, and those melting points are not related to 5-OHU concentration.

A surprising result was that instead of increasing the stability of the triplex, the forming of complex in general decreased its stability. A possible hypothesis is that the complex could be too big so it causes distorted triplex structures. Another possibility is that Cu^{2+} decreases triplex DNA stability. Addition of 5-OHU shielded triplex from the Cu^{2+} effect. However, the errors of these experiments were large, making interpretation of the data difficult.

Table 3.2 Melting temperatures in different Cu^{2+} and 5-OHU concentrations

Cu^{2+} concentration (μM)	**5-OHU concentration (μM)**	**Melting temperature (℃)**	**Standard errors**
2.0	0	42.6	0.5
2.0	0.4	41.2	1.2
2.0	1	42.0	0.71
0.4	0.4	42.9	0.48
1	1	43.2	0.39

A main concern of these experiments was the buffer used for sample incubation. As the phosphates in PBS buffer were good ligands for Cu^{2+}, the free Cu^{2+} concentrations were more diluted than expected. In addition, copper (II) phosphate is not very soluble in water. Copper (II) phosphate may form particles and block or scatter light, which would result in large errors in the measurement. Considering that, in the later work, PBS buffer was removed from the system to examine the influence of buffer to the results of melting tests.

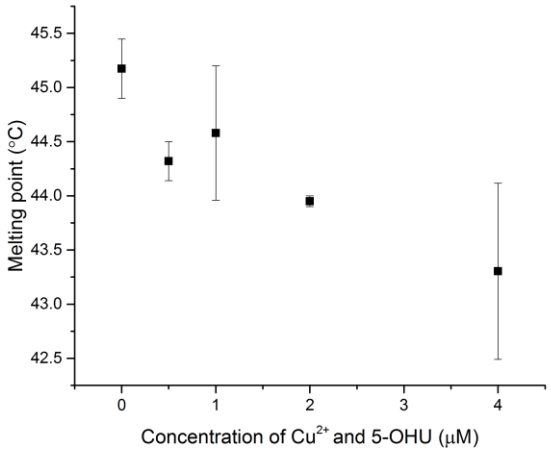

Figure 3.7 UV-vis melting temperatures in the absence of PBS buffer. The system contained 100 nM of A and C strands, 200 nM of B strand, 100 mM of NaCl, 10 mM of $MgCl_2$ and 0.1% SDS (by weight). Cu^{2+} and 5-OHU had the same concentration for all cases.

During the UV-vis melting tests in 100 mM NaCl, 10 mM $MgCl_2$, 0.1% SDS, 100 nM DNA with different Cu^{2+} and 5-OHU concentrations, we found that the melting temperatures were dependent on the concentration of the copper-5-OHU complex. Instead of stabilizing the triplex, the complex destabilized the system. However, destabilization would directly result in purple-to-red color change. This system holds the potential for colorimetric detection of 5-OHU after simple incubation of samples at a certain temperature.

More work needs to be done to understand the binding behavior of the receptor and develop a reliable protocol for simple diagnosis. In the experiment of Figure 3.7, Cu^{2+} concentration was variable because we did not have enough material to study multiple sets of samples with a fixed Cu^{2+} concentration for each set. Otherwise we can suspect that the real reason for triplex destabilization was due to the difference in Cu^{2+} concentrations. We have removed PBS buffers to avoid copper phosphate precipitation. However, that may have resulted in pH-dependent stabilization or destabilization effects. In the future we want to search for a suitable buffer condition, such that the buffer would have less effect on the binding of Cu^{2+} but can maintain the pH. Peter Tlatelpa, a PhD student in our group, demonstrated that increasing the salt concentrations can bring the melting temperature of the triplex-nanoparticle aggregates to above 50 ˚C. When the triplex system has a higher melting temperature, buffer concentration can be at minimal levels to avoid its effect on copper ions.

REFERENCES

1. Adelman, R., Saul, R.L., and Ames, B.N., *Oxidative damage to DNA: relation to species metabolic rate and life span.* Proceedings of the National Academy of Sciences of the United States of America, 1988. **85**(8): p. 2706-2708.

2. Ames, B.N., Shigenaga, M.K., and Hagen, T.M., *Oxidants, antioxidants, and the degenerative diseases of aging.* Proc. Natl. Acad. Sci. USA, 1993. **90**: p. 7915-7922.

3. Thiviyanathan, V., et al., *Base-pairing properties of the oxidized cytosine derivative, 5-hydroxy uracil.* Biochemical and Biophysical Research Communications, 2008. **366**(3): p. 752-757.

4. Tremblay, S., et al., *2'-Deoxycytidine Glycols, a Missing Link in the Free Radical-mediated Oxidation of DNA.* Journal of Biological Chemistry, 1999. **274**(30): p. 20833-20838.

5. Troll, W. and Wiesner, R., *The Role of Oxygen Radicals as a Possible Mechanism of Tumor Promotion.* Annual Review of Pharmacology and Toxicology, 1985. **25**(1): p. 509-528.

6. Kuchino, Y., et al., *Misreading of DNA templates containing 8-hydroxydeoxyguanosine at the modified base and at adjacent residues.* Nature, 1987. **327**(6117): p. 77-79.

7. Poulsen, H., et al., *Detection and interpretation of 8-oxodG and 8-oxoGua in urine, plasma and cerebrospinal fluid.* Biochimica et Biophysica Acta (BBA) - General Subjects, 2014. **1840**(2): p. 801-808.

8. Hoeijmakers, J., *DNA Damage, Aging, and Cancer.* New England Journal of Medicine, 2009. **361**(15): p. 1475-1485.

9. Jackson, S. and Bartek, J., *The DNA-damage response in human biology and disease.* Nature, 2009. **461**(7267): p. 1071-1078.

10. Ames, B.N., Shigenaga, M.K., and Gold, L.S., *DNA lesions, inducible DNA repair, and cell division: three key factors in mutagenesis and carcinogenesis.* Environmental Health Perspectives, 1993. **101**(Suppl 5): p. 35-44.

11. Ashwell, S. and Zabludoff, S., *DNA Damage Detection and Repair Pathways—Recent Advances with Inhibitors of Checkpoint Kinases in Cancer Therapy.* Clinical Cancer Research, 2008. **14**(13): p. 4032-4037.

12. Shigenaga, M.K., et al., *[2] Assays of oxidative DNA damage biomarkers 8-oxo-2'-deoxyguanosine and 8-oxoguanine in nuclear DNA and biological fluids by high-performance liquid chromatography with electrochemical detection,* in *Methods in Enzymology*. 1994, Academic Press. p. 16-33.

13. Sergie, M. and Maxim, F., *H-DNA and Related Structures.* Annual Review of Biophysics and Biomolecular Structure, 1994. **23**(1): p. 541-576.

14. Zhang, Q., et al., *Triple-Stranded DNA Containing 8-Oxo-7,8-dihydro-2'-deoxyguanosine: Implication in the Design of Selective Aptamer Sensors for 8-Oxo-7,8-dihydroguanine.* Analytical Chemistry, 2013. **85**(1): p. 201-207.

15. Huang, H. and Tlatelpa, P.C., *Tuning the selectivity of triplex DNA receptors.* Chemical Communications, 2015. **51**(25): p. 5337-5339.

16. Couchman, P.R. and Jesser, W.A., *Thermodynamic theory of size dependence of melting temperature in metals.* Nature, 1977. **269**(5628): p. 481-483.

17. Lee, J.-S., et al., *A DNA−Gold Nanoparticle-Based Colorimetric Competition Assay for the Detection of Cysteine.* Nano Letters, 2008. **8**(2): p. 529-533.

18. Medley, C.D., et al., *Gold Nanoparticle-Based Colorimetric Assay for the Direct Detection of Cancerous Cells.* Analytical Chemistry, 2008. **80**(4): p. 1067-1072.

19. Daniel, M.-C. and Astruc, D., *Gold Nanoparticles: Assembly, Supramolecular Chemistry, Quantum-Size-Related Properties, and Applications toward Biology, Catalysis, and Nanotechnology.* Chemical Reviews, 2004. **104**(1): p. 293-346.

20. El-Sayed, I.H., Huang, X., and El-Sayed, M.A., *Surface Plasmon Resonance Scattering and Absorption of anti-EGFR Antibody Conjugated Gold Nanoparticles in Cancer Diagnostics: Applications in Oral Cancer.* Nano Letters, 2005. **5**(5): p. 829-834.

21. Storhoff, J.J., et al., *What Controls the Optical Properties of DNA-Linked Gold Nanoparticle Assemblies?* Journal of the American Chemical Society, 2000. **122**(19): p. 4640-4650.

22. Jiang, Y., et al., *A Simple Assay for Direct Colorimetric Visualization of Trinitrotoluene at Picomolar Levels Using Gold Nanoparticles.* Angewandte Chemie, 2008. **120**(45): p. 8729-8732.

23. Lee, J.-S., Han, M.S., and Mirkin, C.A., *Colorimetric Detection of Mercuric Ion (Hg2+) in Aqueous Media using DNA-Functionalized Gold Nanoparticles.* Angewandte Chemie, 2007. **119**(22): p. 4171-4174.

24. Guarise, C., et al., *Gold nanoparticles-based protease assay.* Proceedings of the National Academy of Sciences of the United States of America, 2006. **103**(11): p. 3978-3982.

25. Kalluri, J.R., et al., *Use of Gold Nanoparticles in a Simple Colorimetric and Ultrasensitive Dynamic Light Scattering Assay: Selective Detection of Arsenic in Groundwater.* Angewandte Chemie, 2009. **121**(51): p. 9848-9851.

26. Harada, Y. and Asakura, T., *Radiation forces on a dielectric sphere in the Rayleigh scattering regime.* Optics Communications, 1996. **124**(5–6): p. 529-541.

27. Switzer, C. and Shin, D., *A pyrimidine-like nickel(II) DNA base pair.* Chemical Communications, 2005(10): p. 1342-1344.